Journal of Power Sources 242 (2013) 236–243

Contents lists available at SciVerse ScienceDirect

Journal of Power Sources

journal homepage: www.elsevier.com/locate/jpowsour

In-situ X-ray diffraction study of the phase evolution in undoped and Cr-doped $Li_xMn_{1.5}Ni_{0.5}O_4$ ($0.1 \leq x \leq 1.0$) 5-V cathode materials

W. Zhu [a], D. Liu [a], J. Trottier [a], C. Gagnon [a], A. Mauger [b], C.M. Julien [c], K. Zaghib [a,*]

[a] Energy Storage and Conversion, Research Institute of Hydro-Québec, Varennes, Québec, Canada J3X 1S1
[b] Université Pierre et Marie Curie – Paris 6, Institut de Minéralogie et Physique de la Matière Condensée (IMPMC), 4 place Jussieu, 75005 Paris, France
[c] Université Pierre et Marie Curie – Paris 6, Physicochimie des Electrolytes, Colloïdes et Sciences Analytiques (PECSA), UMR 7195, 4 place Jussieu, 75005 Paris, France

HIGHLIGHTS

- *In-situ* XRD study of the phase diagram of undoped and Cr-doped $LiMn_{1.5}Ni_{0.5}O_4$.
- Comprehensive understanding of the results between previous reports is achieved.
- The off-equilibrium effects and stain effects are analyzed.

ARTICLE INFO

Article history:
Received 23 March 2013
Received in revised form
5 May 2013
Accepted 8 May 2013
Available online 29 May 2013

Keywords:
5-V cathode
LMN
In-situ XRD
Li-ion
Spinel

ABSTRACT

The structural changes of the Cr-doped and undoped $LiMn_{1.5}Ni_{0.5}O_4$ crystallized in the initial disordered phase with space group of $Fd\bar{3}m$ have been investigated during the galvanostatic charge/discharge process at C/24 rate by using *in-situ* X-ray diffraction (XRD) measurements. The de-intercalation of lithium proceeds through a series of first-order phase transitions with two regions of two-phase coexistence. The phase diagram is analyzed and discussed, together with the differences among different results reported in the literature to distinguish between general intrinsic properties of spinel and sample-dependent properties due to deviation from stoichiometry, strain field effects, degree of cation ordering, and out-of-equilibrium effects. We argue that the Cr-doping stabilizes the lattice without impacting the capacity significantly, but decreases the energy density.

1. Introduction

Rechargeable lithium batteries are the most promising power sources for portable electronic devices and electric vehicle applications. Among the lithium containing cathode materials, $LiMn_{1.5}Ni_{0.5}O_4$ (denoted LMN) has been widely studied in the past two decades due to its high operating voltage, (~4.7 V *vs.* Li), high-energy density, low cost and low toxicity [1–5]. Despite all these advantages, the cycling stability of the LMN at high rates still needs to be improved for the practical applications. Therefore, it is important to understand the structure of this material, and its structural changes during cycling in order to improve the material and its properties.

$LiMn_{1.5}Ni_{0.5}O_4$ has a cubic structure, but due to the different Ni and Mn cation distributions in the octahedral sites, two types of spinel structures are observed, namely disordered and ordered LMN, depending on the synthesis conditions. The disordered LMN has a cubic spinel structure with a space group of $Fd\bar{3}m$, where the Ni and Mn ions are randomly distributed at the octahedral 16*d* sites. In contrast, the ordered LMN crystallizes with the $P4_332$ space group, in which the Ni and Mn ions are located in an orderly fashion at the split 4*a* and 12*d* sites [6–10].

The rate capability of lithium extraction/insertion is better in the disordered LMN (S.G. $Fd\bar{3}m$) phase because the electronic conductivity in this phase is several orders of magnitude larger than in the ordered phase [7], and because the diffusivity of lithium ions is higher [10]. The larger electronic conductivity was attributed [7] to the presence of oxygen vacancies in the disordered phase, but it is more likely an intrinsic property. In the stoichiometric composition

* Corresponding author. Tel.: +1 450 652 8019; fax: +1 450 652 8424.
E-mail address: zaghib.karim@ireq.ca (K. Zaghib).

0378-7753/$ – see front matter © 2013 Elsevier B.V. All rights reserved.
http://dx.doi.org/10.1016/j.jpowsour.2013.05.021

of $LiMn_{1.45}Ni_{0.45}Cr_{0.1}O_4$, the cations exist as Ni^{2+} and Mn^{4+}, so that they do not carry the same electronic charge. Therefore, the ordering between Mn and Ni is also a charge ordering that will result in the opening of an electrostatic gap, presumably at the origin of the more insulating character of the ordered phase, even if the presence of oxygen vacancies induces some disorder that can fill partially the energy gap. Moreover, the presence of oxygen vacancies is actually damageable, because this defect results in the presence of Mn in the Mn^{3+} valence state to restore local charge neutrality. Since Mn^{3+} is a strong Jahn–Teller ion, its presence will result in a lattice distortion, weakening the stability and shortening the cycling life of this cathode element. This is consistent with the observation that the distortion of the Mn, Ni(12*d*)-O octahedral site is restrained when the concentration of oxygen vacancies is reduced [3]. For these reasons, a lot of efforts have been devoted to $LiMn_{1.5}Ni_{0.5}O_4$ in the disordered phase without oxygen deficiency [11–14]. Recently, we have succeeded in preparing $LiMn_{1.45}Cr_{0.1}Ni_{0.45}O_4$ samples that satisfy these conditions [4]. First, the substitution of Cr^{3+} for Ni^{2+} and Mn^{4+} helps to keep the Mn^{4+} oxidation state unchanged ($2Cr^{3+} = Ni^{2+} + Mn^{4+}$), but also introduces greater disorder of the B-site cations in LMN [13]. Second, a post-annealing treatment at 600 °C removes the oxygen vacancies and suppresses the Mn^{3+} content, and the voltage plateau at 4.1 V *vs.* Li^+/Li characteristic of the $Li_xNi_{1-x}O$ impurity phase disappears [4].

The phase evolution during lithium de-intercalation/intercalation within these two spinels has been previously studied using both *ex-situ* [15] and *in-situ* [5,16–18] X-ray diffraction techniques. Conflicting results have been reported. In the ordered LMN, three distinct cubic phases were detected relating to each of the Ni^{2+}, Ni^{3+}, and Ni^{4+} oxidation states in the ordered LMN material. These phases transformed from one to another by means of two distinct two-phase regions that correspond to the wide voltage plateaus observed in the electrochemical profile of the cathodes [9,16]. In contrast, the disordered LMN material showed a smooth peak shift to higher angles with no clear two-phase region until nearing the end of charging, which is observed by less pronounced plateaus in the voltage profiles [9,16]. On another hand, a structural change has been reported upon delithiation of disordered $Li_xMn_{1.5}Ni_{0.5}O_4$ at $x = 0.5$ with loss of the glide symmetry [15]. However, a different phase diagram has been reported in Ref. [17] for this same disordered LMN, with a solid solution for large values of x, followed with a two-phase region at $x \sim 0.6$, with the onset of a second cubic phase, phase-2, and another two-phase region at $x < 0.4$, where phase-2 coexists with another cubic phase, phase-3. In Ref. [18], the three phases are found to coexist in a finite range of concentrations. However, the authors did not specify if their measurements were made on ordered or disordered LMN. We can simply note that their result is in agreement with the phase diagram found in Ref. [17] for LMN in the ordered phase, since the three phases are found to coexist only in this case in Ref. [17]. Moreover, the phase diagram is reported to depend on the morphology of the particles [5].

Since the disordered LMN outperforms the ordered LMN as a cathode element for Li-ion batteries, we found desirable to clarify the phase diagram of LMN in the disordered phase. The purpose of this work is to report the study of the structural changes of LMN during lithium extraction and insertion by *in-situ* XRD measurements. Since, in addition, oxygen vacancies have undesirable effects mentioned above, this investigation has been made both on a commercial LMN and the Cr-doped LMN that is free of oxygen vacancy [4]. The differences in phase evolution are compared and the effect of Cr-substitution is discussed.

2. Experimental

The samples used for this study are the same as in our earlier work [4], i.e. the so-called and the same LMN commercial sample from Energy Innovation Group (EIG), Korea; The Cr-doped LMN is the so-called "final $LiMn_{1.45}Cr_{0.1}Ni_{0.45}O_4$ sample". The synthesis process for this last sample has been described in Ref. [4].

To prepare the cathode films, the powders were made into slurries with ~89 wt.% active material, 6 wt.% conductive carbon and 5 wt.% of PVDF binder. The slurries were coated on a 15 μm thick aluminum foil and then dried, cut into 19 mm disks. The *in-situ* XRD patterns were collected from a standard 2032 coin-cell (as depicted in Fig. 1) in which a 0.1-μm thick Al foil was used as window for the XRD beam and current collector for the cathode. A 10 mm hole was drilled on the top case of the cell for the X-ray to pass through. A cathode film was put into the case with the aluminum collector facing the hole. Silver epoxy was used to seal the top case with aluminum. The *in-situ* X-ray measurement was performed on a Bruker D8 Advance diffractometer with Cu-kα radiation. The data were collected every two hours with scan-step size 0.025°. The sample displacements were corrected by taking aluminum diffraction peaks as reference. The as-made films were also characterised by X-ray diffraction, with same step size but longer data-collect time in order to collect all the peaks, especially the weak ones.

The electrochemical cells consist of an LMN cathode, a separator (Celgard 3501), a Li counter electrode and electrolyte which is a mixture of 1 mol L^{-1} $LiPF_6$ dissolved in ethylene carbonate–dimethyl carbonate (1:1 v/v). The cathode loadings are 28.747 mg and 14.753 mg for LMN and Cr–LMN electrodes, respectively. All the components were dried at 80–120 °C overnight under vacuum and then assembled in an argon-filled glove box. The electrochemical measurements were carried out on Biologic SP300 (Bio-Logic Science Instrument), controlled by EC-Lab (V10.19), between 3.5 and 4.9 V. The experimental coin-cells were first cycled at C/12 rate to activate the cathode materials, and then cycled at lower rate of C/24, where all the XRD data were collected.

3. Results and discussion

3.1. Structural analyses of the electrode films

Fig. 2 shows the XRD patterns of the undoped and Cr-doped LMN cathode films deposited onto an aluminum foil used as

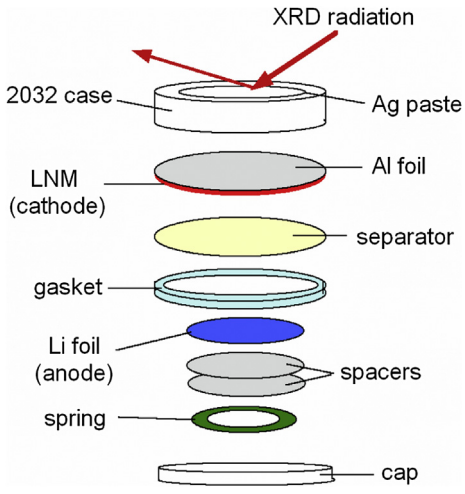

Fig. 1. Schematic diagram of the experimental coin-cell configuration.

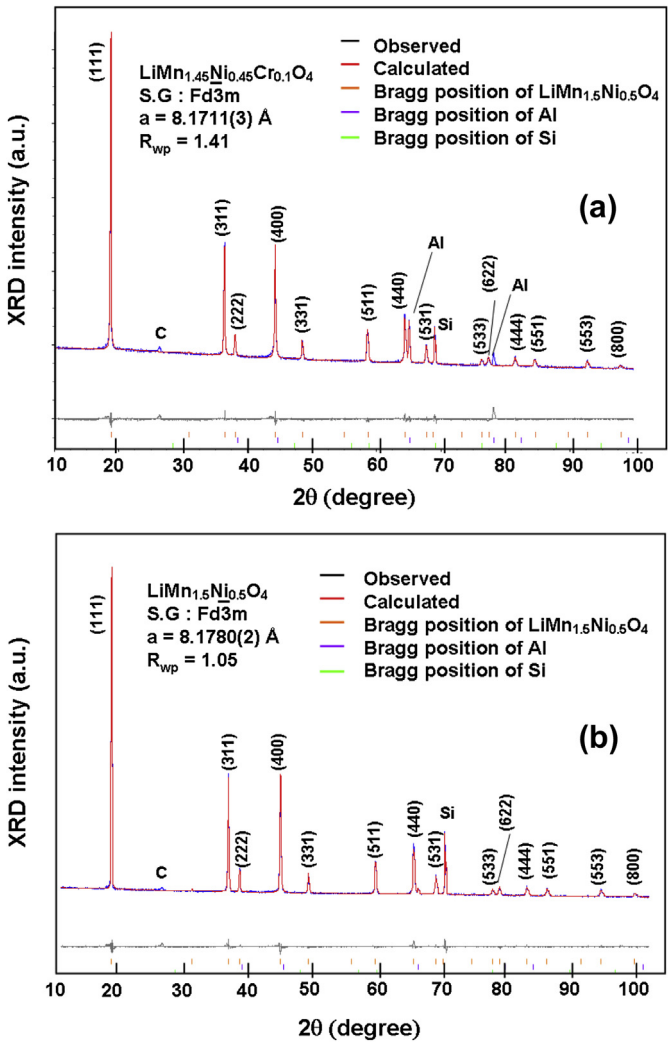

Fig. 2. Rietveld refinement profiles of the XRD data for the (a) Cr-doped LMN and (b) commercial LMN electrode films (Si peak comes from sample holder).

current collector, and the Rietveld refinements in the $Fd\bar{3}m$ space group. No superstructure peaks were detected at $2\theta = 15.3°$, 39.7°, 45.7°, 57.5°, and 65.6°, which are the positions representing an ordering of the Ni(II) and Mn(IV) ions in the $P4_332$ spinel structure [19]. Therefore, both the undoped and Cr-doped LMN are crystallized in the $Fd\bar{3}m$ disordered phase. In addition, none of the films exhibits Bragg lines at ca. $2\theta = 18.8°$ and 44.3° that are those of the $Li_{1-x}NiO$ impurities, in agreement with our previous result [4]. Moreover, all the diffraction peaks can be indexed in the space group $Fd\bar{3}m$ (JCPDS No. 80-2162) of a cubic spinel. In our previous work [4], we deduced from the analysis of the Fourier transform infrared (FTIR) experiments that the cation disorder is stronger in the Cr-doped sample than in the undoped one, "stronger disorder" being understood in terms of Ni^{2+}, Mn^{4+} cations ordered on the octahedral sites at shorter range only [4].

The Rietveld refinement of the Cr-doped LMN in Fig. 2 has been obtained gives the lattice parameter $a = 8.1711(3)$ Å corresponding to a volume of the unit cell $V = 545.57$ Å^3 with the Rietveld parameters $R_{wp} = 1.41$, $R_{ex} = 0.63$ and $R_p = 0.87$. The lattice parameter is smaller than that of the commercial sample ($a = 8.1780(2)$ Å, $V = 546.94(6)$ Å^3, $R_{wp} = 1.05$, $R_{ex} = 0.63$, $R_p = 0.69$). Since the ionic radius of Mn^{4+} (0.54 Å) is smaller than that of Mn^{3+} (0.66 Å), it is reasonable to assume that most of the residual Mn^{3+} ions in $LiMn_{1.45}Ni_{0.45}Cr_{0.1}O_4$ have been re-oxidized to Mn^{4+} after re-annealing at 600 °C [4].

3.2. Phase evolution during the electrochemical process

Fig. 3 compares the typical charge/discharge curves of the two samples recorded at a low current density of C/24 rate. At first glance, there are only minor differences between the two cells. For example, undoped LMN shows a little higher voltage plateaus than those of the Cr-doped spinel. Additionally, Cr-doped LMN exhibits two distinct plateaus at around 4.7 V. This result corresponds to the two peaks of the differential capacity curves reported in Fig. 11 of Ref. [4]. The undoped LMN only shows a relatively flat voltage profile. This is due to the fact that the difference in voltage between the two plateaus is smaller, so that the existence of the two plateaus in that case is better evidenced by the differential capacity curves reported in Ref. [4]. The average potential difference, ΔV, between these two plateaus in Fig. 3 (or equivalently to the two peaks in Fig. 11 of Ref. [4]) is ca. 60 mV for the Cr-doped LMN material and 30 mV for the commercial sample, which reflects the stronger cation disorder of the Cr-doped sample [4]. The shift between the anodic and cathodic peaks is ~26 mV for the Cr-doped sample, against ~65 mV in the undoped LMN. This smaller hysteresis in the Cr-doped sample is consistent with the faster Li-diffusivity in the disordered phase [10], confirmed by the increase of the rate capability at high C-rate for the Cr-doped sample [4]. Both the oxidation and reduction plateaus are shifted toward lower voltage for the Cr-doped LMN with respect to those of the undoped LMN, by ~30 mV. Kim et al. [9–15] have pointed out that the lithium ions require more energy to be intercalated/de-intercalated from the host structure of ordered $LiMn_{1.5}Ni_{0.5}O_4$, leading to a higher redox potential. Therefore, this 30 mV shift can also be ascribed to the longer range of cation ordering in the undoped LMN cathode, confirmed by the infrared spectroscopy measurements on these samples [4]. In addition, while the manganese in the Mn^{4+} valence state in stoichiometric LMN, the oxygen vacancies generate Mn^{3+} as a result of the charge compensation. The presence of Mn^{3+} in the samples can be detected by the voltage plateau at the redox potential circa 4.0 V of Mn^{3+}/Mn^{4+} *versus* Li^+/Li. This feature is well detected in the charge/discharge curves of the undoped sample, but is barely detectable for the Cr-doped sample. Therefore, the concentration of oxygen vacancies is significantly smaller in the Cr-doped sample that is close to stoichiometry, which confirms this

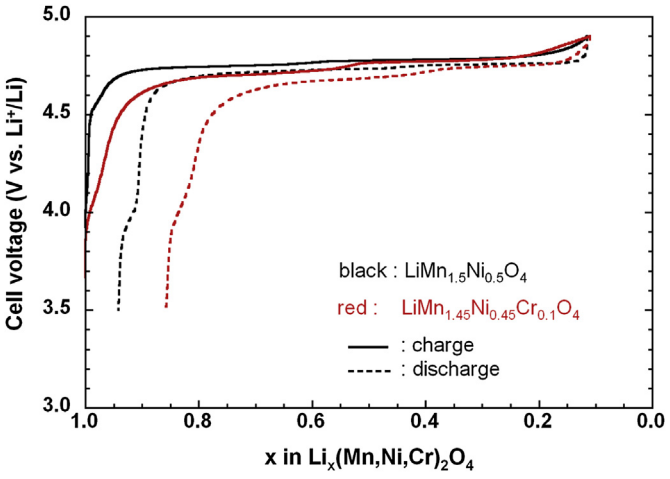

Fig. 3. Charge/discharge curves of the Cr-doped LMN and commercial LMN samples measured at C/24 rate.

result deduces from the analysis of the magnetic properties in Ref. [4].

The evolution of *in-situ* XRD patterns of both electrode films during the cycling at C/24 rate is reported in Fig. 4. In order to better understand the phase evolution, two diffraction peaks, (311) in the range $2\theta = 35.5–38^\circ$ and (511) in the range $2\theta = 58–60.5^\circ$ have been selected because they have the minimum overlap with the Bragg line of the Al current collector. Fig. 5 compares the evolution of these (311) and (511) diffraction peaks for the undoped and Cr-doped LMN during the charge process. Overall, all the diffraction peaks shifted to the higher 2θ angles as the lithium ions were removed from the two host structures. The analysis of the XRD pattern shows that all the phases are cubic, and the lattice parameters for each phase as a function of x deduced from the least-squares fitting of the XRD spectra measured over one charge–discharge cycle are reported in Fig. 6a and b for the Cr-doped and the undoped sample, respectively. The proportion of the different phases during the full cycle is reported in Fig. 7 for both samples for comparison.

Let us first analyze the data for the Cr-doped sample. As charge proceeds from $x = 1$, we first observe a solid solution in the whole range $1 \leq x \leq 0.72$, the decrease in Li resulting only in the decrease of the lattice parameter of the cubic phase that we label as phase-1. A new cubic spinel phase (phase-2) started to emerge and the system thus undergo a first-order transition at $x = 0.72$, to enter in a two-phase domain $0.72 \leq x \leq 0.54$, in which the phase-2 grows at the expense of the phase-1, so that the phase-1 disappears at the Li concentration $x = 0.54$. Below this concentration, we find a small but finite range of concentration $0.54 \leq x \leq 0.37$, in which the Cr-doped is again a solid solution in the phase-2 only. The system re-enters a two-phase region in the range $0.37 \leq x \leq 0.13$ with the coexistence of phase-2 and a new phase (phase-3) that grows at the expense of phase-2. Finally, a solid solution with phase-3 only is observed in the range $x \leq 0.13$. The experimental XRD spectra have been measured along the cycle with steps $\Delta x \sim 0.1$, so that the uncertainty in the estimates of the Li concentrations of the phase boundaries can be estimated to ± 0.05. Upon discharge, phase-3 is found to be a solid solution up to $x = 0.25$. This result gives evidence that, even at the low C-rate of the experiment, thermodynamic equilibrium at the end of the charge was not reached. At the end of charge a very small faction (few % only) of phase-2 is still detectable. However, during the period of time that the sample has been let in open-circuit before the cell is discharge, this phase-2 has been converted in phase-3 only, as it can be seen in Fig. 7. This can also be seen as the discontinuity between the end of discharge and the beginning of charge in Fig. 6. Therefore, at equilibrium, the Cr-doped sample will be in a solid solution in phase-3 at low values of $x \leq 0.25$. Upon discharging, the phase-2/phase-3 system is found in the range $0.26 \leq x \leq 0.43$. The difference between 0.37 and 0.43 does not exceed the experimental uncertainty and is thus negligible. The onset of phase-1 in phase-2 is also the same at charge and discharge. Therefore, within this experimental uncertainty, we can deduce that the phase transformations are totally reversible, without any hysteresis, except for a small shift concerning the limit in the solid solution in phase-3 that, however, is not an intrinsic effect, and clearly an artefact due to deviation from equilibrium.

The phase diagram for the undoped sample is qualitatively the same. Upon charging, the phase diagram is the same down to $x = 0.5$. The phase-1 upon charging persists down to $x = 0.46$ against 0.54 in the Cr-doped sample, a difference that is still within the experimental precision. The phase-3 sets up at this concentration, while it starts only at 0.42 in the Cr-doped sample, so that there is no region where only the phase-2 is observed. The absence of solid solution in phase-2, however, is again likely due to the

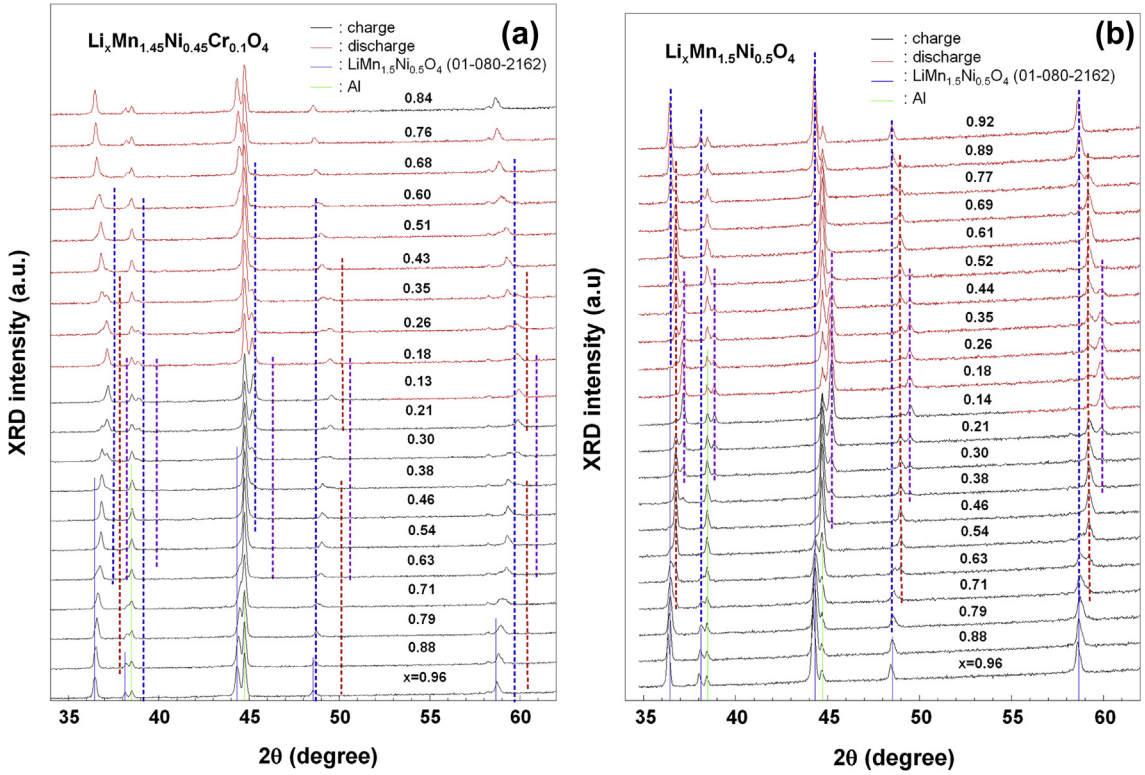

Fig. 4. *In-situ* XRD patterns of the (a) Cr-doped LMN and (b) undoped LMN, as a function of the Li concentration x during the galvanostatic cycling. The dotted lines are drawn for the guidance of eyes to view the three different phases, in blue, red and purple for the phases-1, -2, -3, respectively on the web version. (For interpretation of the references to colour in this figure legend, the reader is referred to the web version of this article.)

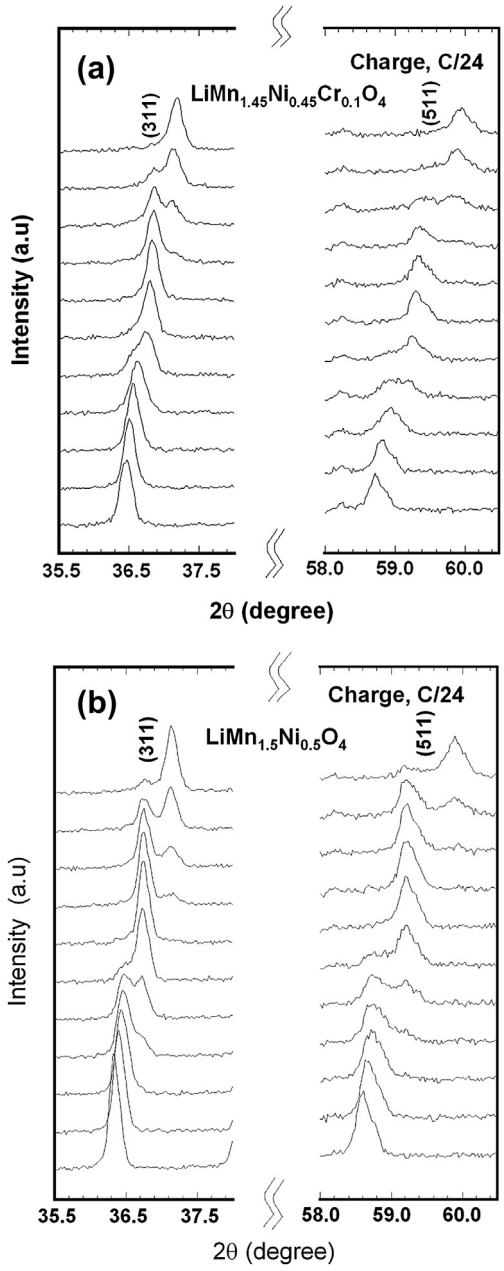

Fig. 5. *In-situ* XRD patterns of the (311) and (511) peaks of (a) Cr-doped LMN and (b) undoped LMN spinels during cycling at C/24 rate.

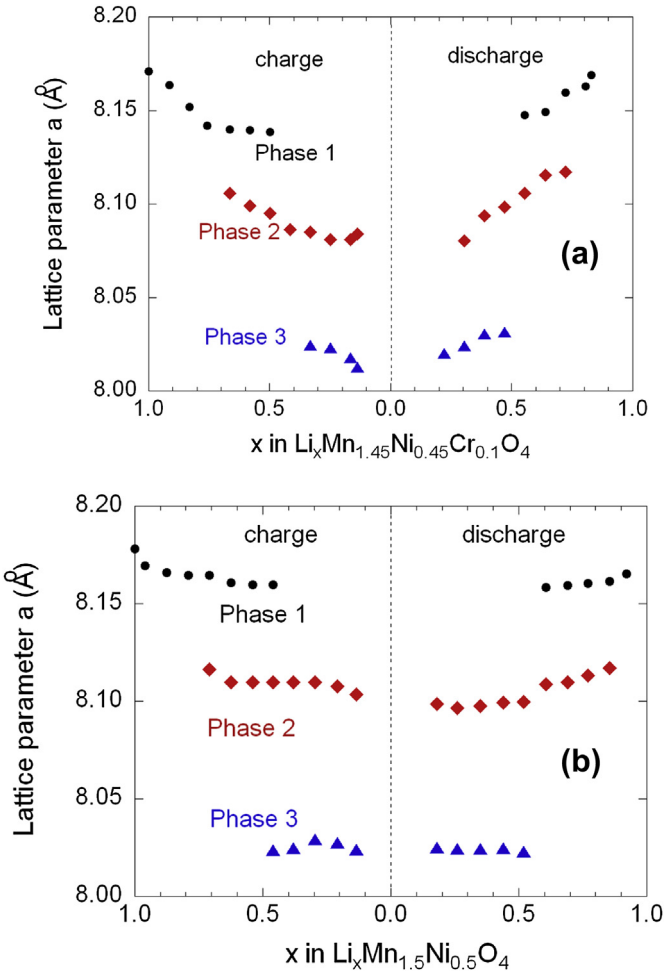

Fig. 6. Variation of the lattice parameters of the different cubic phases in the Cr-doped sample (a) and the undoped sample (b) as a function of the Li concentration x during the charge (a) and discharge (b) during cycling at C/24 rate.

out-of-equilibrium of the cell at the end of charge, because, upon discharge, this solid solution is again observed in the range $0.51 \leq x \leq 0.60$. This is confirmed by the larger amount of phase-2 that is detected at the end of charge in the undoped sample than in the Cr-doped sample as it can be seen in Fig. 7. We can also see in this figure that the phase-2 has shrunk during the period of time in open-circuit before the discharge (1 min), but slowly so that there is still a small but finite proportion of the undoped LMN in this phase-2 at the beginning of the discharge.

4. Discussion

To understand the link between the phase diagram that we have determined in the previous section and the electrochemical properties, we have reported in Fig. 8 the variation of the voltage with x for the two samples, together with the range of existence of the different phases. First, we observe that the voltage of the battery with the Cr-doped sample is smaller than with the undoped sample at any Li concentration x, except in the small region $0.1 \leq x \leq 0.2$. The unexpected larger value of the voltage in this small region is clearly attributable to the fact that a larger proportion of phase-2 is still observed in the undoped sample in this range of concentration. Since the voltage associated to the phase-2 is lower that of phase-3, the persistence of this phase lowers the potential, which becomes lower than in the Cr-doped sample where only the phase-3 is observed. We also note that the voltage is strongly dependent of the composition in this small range of composition. This is true for the case of the Cr-doped sample, and this is expected since the Cr-doped sample is a solid solution in phase-3. In case of a two-phase regime, however, the Gibbs rule tells us that $V(x)$ should be a flat plateau, while the potential varies very fast with x in this region. Therefore, the strong variation of $V(x)$ in the undoped sample in the small range $0.1 \leq x \leq 0.2$ confirms that it is not in a two-phase regime. Instead, it should be considered as a solid solution in phase-3. The presence of the phase-2 simply means the existence of some isolated phase-2 clusters attributable to the difficulty to reach thermodynamic equilibrium. The slower dynamics in this undoped sample is due to the fact that the local cation ordering is larger than in the Cr-doped sample [4], which results in a smaller Li-diffusivity [10]. This is also confirmed by the

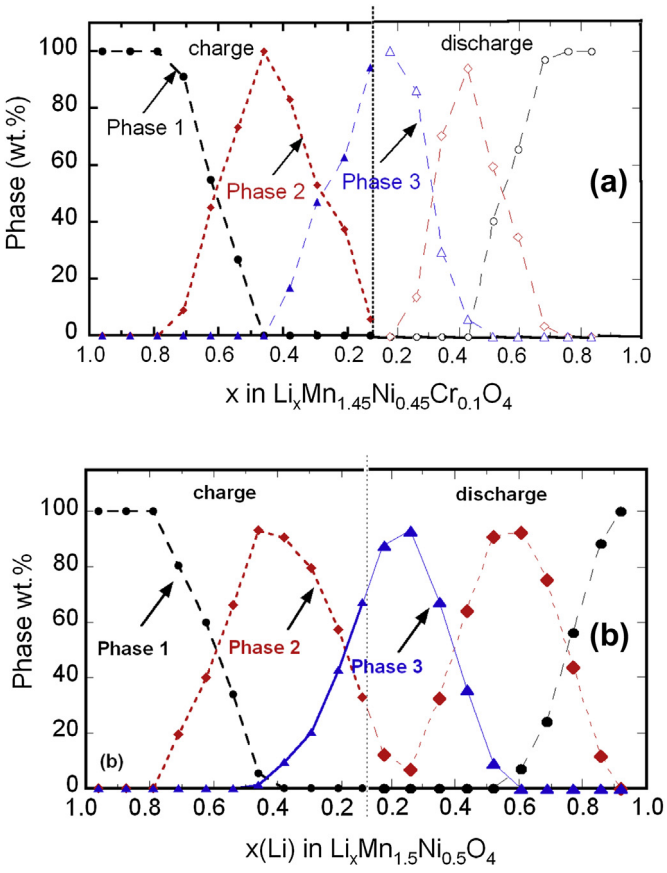

Fig. 7. Relative concentrations of the different cubic phases in the Cr-doped (a) and undoped (b) samples as a function of the Li concentration x during a cycle at C/24 rate.

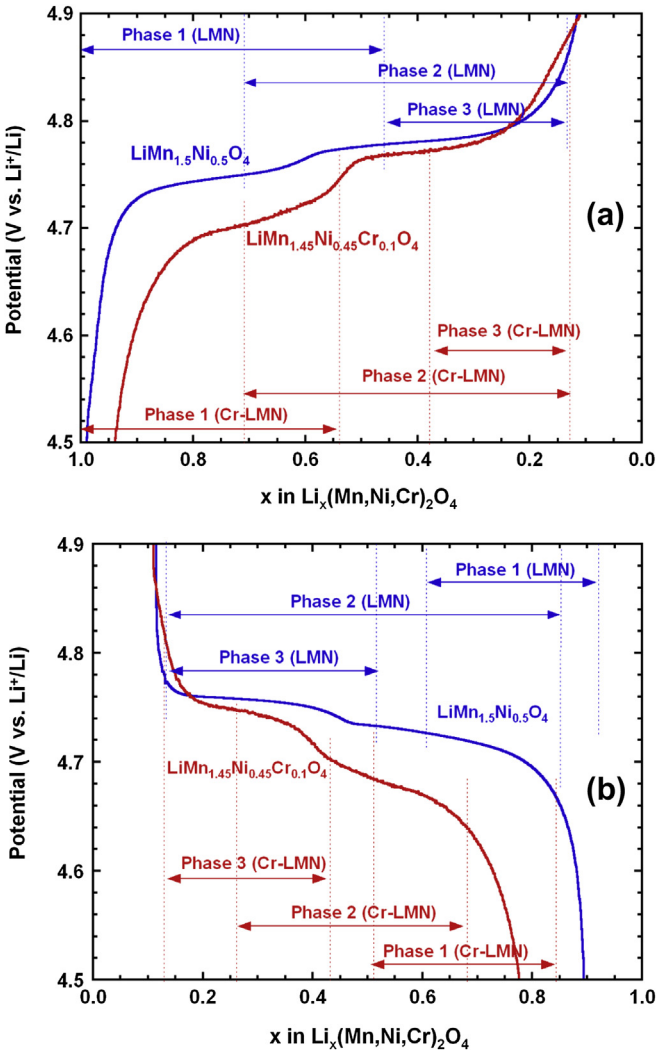

Fig. 8. Variation of the voltage as a function of the Li concentration x during charge (a) and discharge (b) in a cycle at C/24 rate as a function of x(Li) in Cr-doped and undoped samples in relation to the phase diagram.

smaller capacity retention of the undoped sample at high C-rate [4]. Basically, the local ordering detected by the infrared spectroscopy [4] for the commercial sample may reduce the mobility of the interface between phase-2 and phase-3 domains, which generates this out-of-equilibrium situation where phase-2 isolated clusters still exist at the end of discharge, in a larger proportion in the case of the undoped sample, according to Fig. 8. This effect also implies that the presence of phase-2 domains at such small concentrations of lithium is not an intrinsic property and is thus sample dependent. Indeed, the same effect in disordered LMN has been observed in Ref. [11], but not in Ref. [5]. The fact that there is a difference between charge and discharge curves in Fig. 8 gives other evidence that the thermodynamic equilibrium was not reached during the experiments, despite the slow C-rate chosen for the experiments for the undoped sample, but also to a smaller extent for the Cr-doped sample. In particular, for the Cr-doped sample, the coexistence of phase-2 and phase-3 at small x during charge, and only phase-3 for $x < 0.2$ in agreement with the result obtained during charge–discharge at C/18 rate in ordered LMN particles of octahedral shape [5] with approximately the shape of the particles in the present work [4] but bigger (2 μm in size in Ref. [5] against 500 nm here [4]), and also in cation-disordered LMN plates. The off-equilibrium effects evidenced by hysteresis in the structure and electrochemical properties between charge and discharge as a function of x for the Cr-doped sample are also linked to its larger cation disorder. Indeed, we know from the general physics of disorder phenomena that disorder is responsible for a slowing of the dynamics, evidenced by the divergence of the viscosity in glasses, or the critical slowing-down at the approach of the spin glass transition in diluted magnetic materials, for instance.

Let us now consider the phase diagram for $x > 0.2$. The first striking result is that the Cr-doping reduces the potential of the battery, which can be attributed to an inductive effect [20], implying that the Cr-doping strengthens the Ni–O bond. This is consistent with the fact that the Cr-doping allowed us to increase the cation disorder without loosing oxygen [4], while disorder in the undoped LMN increases the oxygen deficiency.

Since the phase diagrams between the two samples show small difference, we shall discuss only the results obtained on the Cr-doped sample. The existence of the three phases with first-order transitions to two phases regions separated by solid solutions has already been observed and extensively studied in $Li_xMn_2O_4$ [21]. It is then characteristic of spinels. Phase-1 extends from $x = 1$ up to $x = 0.54$ in our case. This range is markedly different from the result in Ref. [5] where it extends down to $x = 0.3$. On another hand, our result is in agreement with that of Kim et al. [9] for a stoichiometric undoped sample, while an extension of the phase-1 down to $x = 0.3$ was observed only for a sample that was deficient in oxygen. In addition, the extension down to $x = 0.3$ in Ref. [5] was obtained not only for the octahedral particles in the more ordered phase, but also for the plates where the cation ordering is reduced importantly. The oxygen deficiency is thus a pertinent parameter

that determines the extension of phase-1, rather than the degree of cation ordering. The phase-1 is a solid solution only in the range $1.0 \leq x \leq 0.72$, before it undergoes a first-order transition of a two-phase region phase-1/phase-2. This is again in agreement with the result found for the stoichiometric sample in Ref. [9] and the octahedron-like particles in Ref. [5] during charge, but not the plates in Ref. [5] where phase-1 is a solid solution down to $x = 0.3$. Nevertheless, the results should be compared to the plates rather than the octahedra, because the cation disorder in the octahedra is small. The difference in the extension of the solid solution in phase-1 is thus significant. To explain this behavior, one has to consider the general theory of sorption in nano-porous media [22], in particular the effect of lateral force on the adsorption. Bazant and Bazant [22] have treated this problem to explain the puzzle of sorption hysteresis of water in cement concrete or cement paste, but the mapping to the present case can be made. The result is that, due to attractive lateral interactions, (say a strain field in our case) the homogeneous free energy of mixing of the adsorbate molecules (Li in the occurrence) becomes non-convex and leads to at least two local minima in the total free energy, corresponding to stable high-density (Li-rich) and low-density (Li-poor) adsorbed phases, thus giving rise to the classical picture of the appearance of a miscibility gap. The strain field is one of the properties that depend on the samples because it depends on the local structural properties, which may explain the differences between the phase diagrams reported in the Li-spinels, either LMN or $LiMn_2O_4$, during cycling, and a shift in the transition between the solid solution in phase-1 and the two-phase region phase-1/phase-2 from 0.3 to 0.7 depending on the authors. Indeed, this sensitivity to local cation ordering and stoichiometry is particularly important in the solid solution of spinels [23].

In this scheme, the demixion in a two-phase system is thus different from the case met in $LiFePO_4$ for instance, where the phase separation originates from the Coulomb correlations inside the material [24], in which case the phase diagram is robust [25]. There is, however, one basic difference between the sorption–desorption of water in concrete and that of lithium in the spinel. In the former case, the variable in the experiments is the humidity, not the filling factor, and the hysteresis investigated is the difference of the humidity at which the demixion takes place when the humidity increases or decreases, depending on the humidity sweep rate. In our problem, the role of humidity should be the C-rate, which is constant during the experiment, and the variable is the lithium concentration, i.e. the filling factor. The model in Ref. [22] explains that the difference between the phase diagrams measured at different C-rates. In addition, the hysteresis is increased by non-equilibrium phenomena, evidenced by over-potential in Li-ion batteries. That is why the phase diagram depends importantly on the C-rate that is used in the experiments, and the reason why we have chosen a low (C/24) rate; this is also the reason why we limit the comparison between our experiments with data available in the literature at comparable low C-rate to be as close as possible to thermodynamic equilibrium. In this case, the hysteresis between the Li concentrations between solid solutions and two-phase systems measured during charge and discharge essentially results from the delay in phase separation due to either nucleation or spinodal decomposition, which is small. Nevertheless, we have given evidence that, even at C/24 rate, equilibrium has not been reached, which explains that the results can be quantitatively different, since none of the experiments have been performed at the same C-rate. A common feature in the present work and the prior results reported in the literature, however, is the full reversibility between charge and discharge for the samples in the $Fd\bar{3}m$ phase, contrary to the case of LMN in the ordered phase, with small hysteresis phenomena only. This is verified for both the Cr-doped and undoped LMN samples. In particular, even if equilibrium has not been reached at C/24 just at the end of the cycle, the equilibrium will be reached afterwards, so that, at the end, the battery does not age (at least at the scale of 100 cycles), even at faster C-rate in our Cr-doped sample [4].

It is commonly admitted that each phase is correlated with a different oxidation state of nickel ions. In this picture, phase-2 is associated to the phase where all Ni^{2+} are converted in Ni^{3+}, i.e. the phase $Li_{0.5}Mn_{1.5}Ni_{0.5}O_4$. In the Cr-doped sample, it means $Li_{0.45}Mn_{1.45}Cr_{0.1}Ni_{0.45}O_4$. Actually, at these Li concentrations, the samples are in phase-2 (except in some cases for a residual concentration of phase-1). In the same way, $Li_{0.1}Mn_{1.5}Ni_{0.5}O_4$ and $Li_{0.1}Mn_{1.45}Cr_{0.1}Ni_{0.45}O_4$ are in phase-3 at equilibrium, and correspond to the case where all the nickel ions have been converted to Ni^{4+}, since the chromium will not be active in the range of potentials that we have investigated. Nevertheless, the lattice parameter varies as a function of x (see Fig. 6), in particular for phases-1 and phase-2. This feature, which is also met in $Li_xMn_2O_4$ where it makes difficult the determination of the composition of the phases [21], is unexpected for a truly two-phase system where only the proportion of the two phases should vary with x, not the composition of each phase. This can be understood as an evidence of a thick interface between the two phases in the two-phase regime, especially for the phases-1 and -2. In other words, the lithium density does not change abruptly at the interface, but changes gradually over a certain distance between the two phases. This structural model is called a pseudo- or non-ideal two-phase structure [26]. In particular, if the size of a domain is small so that the surface over volume ratio is not small, the lattice parameter deduced from the XRD analysis will affected by the interface, and will differ from the Li concentration in the core region. Incidentally, if the two phases have different equilibrium volumes, then elastic coherency strain energy further reduces the miscibility and spinodal gaps, and can eliminate phase separation [27], which implies that the Li-composition of the clusters may even depend on their size and thus on the relative proportion of the two phases. This is consistent with the fact that the "plateaus" in Fig. 8 are not flat. This is again a major difference with $LiFePO_4$ that is a truly two-phase system, as it is evidenced by the broad plateau at 3.5 V in the charge–discharge curves, in this compound. The paradox is then that the spinels might be a realization of the model in Ref. [27] that was originally applied to $LiFePO_4$.

Although the differences between the undoped and Cr-doped samples are small, we can observe in the phase-1 that the variations of the lattice parameter with x are larger in the Cr-doped case. Actually the stronger variation is an evidence of the stronger cation disorder, as the lattice parameter varies with x in the $Fd\bar{3}m$ case, while it remains almost constant in the phase-1 of the $P4_332$ case [9,16,17]. This is consistent with our previous results [4] and other works as well [12,28] showing that Cr-substitution increases the disordered structure within the $LiMn_{1.5}Mn_{0.5}O_4$ spinel lattice.

This lager variation of the lattice parameters of the different cubic phases with x in the Cr-doped sample also gives enlightenment on another result in Ref. [4], namely the much larger peak value in the differential capacity curves of the undoped sample. Indeed, when the lattice parameter changes, so does the redox potentials associated to the nickel, so that the voltage plateau is no longer flat, which decreases the peak values in Fig. 11 of ref. [4] for this sample.

The charge–discharge curves in Fig. 8 give additional information on the effect of the Cr-doping on the performance of LMN. We have already mentioned that the full conversion of Ni^{2+} to Ni^{4+} is achieved in $Li_{0.1}Mn_{1.45}Ni_{0.45}Cr_{0.1}O_4$, so that we might expect a loss of capacity since 0.1 Li remains, while full delithiation might be obtained in the undoped sample. In practice, however, we find that the potential of the two cells reaches 4.9 V at $x = 0.1$, which is the

potential where the charge is stopped to protect the electrolyte. Therefore, as long as we cannot use electrolytes that extend the electrolyte window to larger potentials, the amount of lithium that can be removed from the undoped and Cr-doped samples are the same, i.e. the available capacity is the same. This is due to the inductive effect that lowers the potential of the Cr-doped sample, which has another advantage, namely an increase of the safety. Indeed, Huggins [29] has shown that the partial pressure of oxygen increase very fast with the voltage in oxides of transition metals, so that high voltage favours the loss of oxygen, which explains the difficulty to prepare stoichiometric LMN. Indeed, this result shows that the Cr-doping stabilizes the oxygen inside the material. Moreover any loss of oxygen implies safety hazard, especially with graphite anode, since the oxygen liberated from the cathode will interact with the carbon anode and the exothermic reaction converting the carbon in CO_2 will be responsible for thermal runaway. Therefore, by stabilizing the lattice, the Cr-substitution also increases the safety of the battery. The only drawback will be a loss of energy density associated to the lower operating voltage.

5. Conclusion

In this work, we have investigated the structural evolution of a $Li_xMn_{1.45}Ni_{0.45}Cr_{0.1}O_4$ sample and a commercial $LiMn_{1.5}Ni_{0.5}O_4$ in the $Fd\bar{3}m$ phase as a function of the Li content (x) using *in-situ* XRD analyses. Results of both charge (Li extraction) and discharge (Li insertion) reactions have been reported in order to better understand the influence of Cr-substitution to the spinel. The phase diagram for both samples shows the existence of three phases that form alternatively solid solutions and two-phase regions. The results have been understood on a basis of a model that takes strain effects into account, also explaining the fact that the phase diagram is sample dependent, differs between the different results reported in the literature. The analysis of the phase diagram confirms the faster dynamics of the Li-insertion/de-insertion in the Cr-doped sample, evidenced by the improved capacity retention at high C-rates. The other benefit of the Cr-substitution is the increase of the stability of the lattice. The drawback is a decrease in the energy density that is not due to a loss of capacity, but a smaller redox potential of the nickel *vs.* Li^+/Li.

Acknowledgments

The authors are pleased to acknowledge the support from the U.S. Department of Energy under the BATT program (with Lawrence Berkeley National Laboratory).

References

[1] Q. Zhong, A. Bonakdarpour, M. Zhang, Y. Gao, J.R. Dahn, J. Electrochem. Soc. 144 (1997) 205.
[2] K. Amine, H. Tukamoto, H. Yasuda, Y. Fujita, J. Power Sources 68 (1997) 604.
[3] Y. Idemoto, H. Narai, N. Koura, J. Power Sources 119 (2003) 125.
[4] D. Liu, J. Hamel-Paquet, J. Trottier, F. Barray, V. Gariépy, P. Hovington, A. Guerfi, A. Mauger, C.M. Julien, J.B. Goodenough, K. Zaghib, J. Power Sources 217 (2012) 400.
[5] B. Hai, A.K. Shukla, H. Duncan, G. Chen, J. Mater. Chem. A 1 (2013) 759.
[6] N. Amdouni, K. Zaghib, F. Gendron, A. Mauger, C.M. Julien, Ionics 12 (2006) 117.
[7] M. Kunduraci, J.F. Al-Sharab, G.G. Amatucci, Chem. Mater. 18 (2006) 3585.
[8] K. Takahashi, M. Saitoh, M. Sano, M. Fujita, K. Kifune, J. Electrochem. Soc. 151 (2004) A173.
[9] J.-H. Kim, S.-T. Myung, C.S. Yoon, S.G. Kang, Y.-K. Sun, Chem. Mater. 16 (2004) 906.
[10] T. Minami, M. Tatsumisago, M. Wakihara, C. Iwakura, S. Kohjiya, I. Tanaka (Eds.), Solid State Ionics for Batteries, Springer-Verlag, Tokyo, 2005, p. 101.
[11] T.A. Arunkumar, A. Manthiram, Electrochim. Acta 50 (2005) 5568.
[12] G.B. Zhong, Y.Y. Wang, Y.Q. Yu, C.H. Chen, J. Power Sources 205 (2012) 385.
[13] D. Liu, Y. Lu, J.B. Goodenough, J. Electrochem. Soc. 157 (2010) A1269.
[14] D.W. Shin, A. Manthiram, Electrochem. Commun. 13 (2011) 121.
[15] J.-H. Kim, C.S. Yoon, S.-T. Myung, J. Prakash, Y.-K. Sun, Electrochem. Solid-State Lett. 7 (2004) A216.
[16] M. Kunduraci, G.G. Amatucci, J. Electrochem. Soc. 153 (2006) A1345.
[17] L. Wang, H. Li, X. Huang, E. Baudrin, Solid State Ionics 193 (2011) 32.
[18] K. Rhodes, R. Meisner, Y. Kim, N. Dudney, C. Daniel, J. Electrochem. Soc. 158 (2011) A890.
[19] R. Alcantara, M. Jaraba, P. Lavela, J.L. Tirado, Chem. Mater. 15 (2003) 2376.
[20] A. Padhi, K. Nanjundaswamy, C. Masquelier, S. Okada, J.B. Goodenough, J. Electrochem. Soc. 144 (1997) 1609.
[21] X.Q. Yang, X. Sun, S.J. Lee, J. McBreen, S. Mukerjee, M.L. Daroux, X.K. Xing, Electrochem. Solid-State Lett. 2 (1999) 157.
[22] M.Z. Bazant, Z.P. Bazant, J. Mech. Phys. Solids 60 (2012) 1660.
[23] E. Lee, K.A. Persson, Energy Environ. Sci. 5 (2012) 6047.
[24] F. Zhou, A.C. Marianetti, M. Cococcioni, D. Morgan, G. Ceder, Phys. Rev. B 69 (2004) 201101.
[25] K. Zaghib, A. Guerfi, P. Hovington, A. Vijh, M. Trudeau, A. Mauger, J.B. Goodenough, C.M. Julien, J. Power Sources 232 (2013) 357.
[26] Z.G. Chai, C.F. Meng, J. Appl. Cryst. 31 (1998) 7.
[27] D.A. Cogswell, M.Z. Bazant, ACS Nano 6 (2012) 2215.
[28] D.W. Shin, C.A. Bridges, A. Huq, M.P. Paranthaman, A. Manthiram, Chem. Mater. 24 (2012) 3720.
[29] R.A. Huggins, J. Electrochem. Soc. 160 (2013) A3001.